

Highlights

A mechanical model for reinforced, expanding spirally-wound layered materials

Robert Timms, Steven Psaltis, Colin P. Please, S. Jon Chapman

- Research highlight 1
- Research highlight 2

A mechanical model for reinforced, expanding spirally-wound layered materials

Robert Timms^{a,b,*}, Steven Psaltis^c, Colin P. Please^{a,b}, S. Jon Chapman^{a,b}

^a*Mathematical Institute, University of Oxford, Andrew Wiles Building, Woodstock Road, Oxford, OX2 6GG, UK*

^b*The Faraday Institution, Quad One, Becquerel Avenue, Harwell Campus, Didcot, OX11 0RA, UK*

^c*School of Mathematical Sciences, Queensland University of Technology, Brisbane, QLD 4000, Australia*

Abstract

Mechanical deformations induced by expansion within an elastic material which is spirally-wound in layers with a thin inextensible reinforcing material are considered. The motivation is to understand behaviour of spirally-wound batteries where both the active material and the metal current collectors expand due to changes in lithiation and/or temperature. This paper considers a spiral made from a single reinforcing layer with a matrix layer of linear elastic material, whose properties may vary through the layer. The layers undergo prescribed isotropic expansion, where the matrix expansion may depend on the macroscopic radial coordinate. Asymptotic homogenisation, exploiting the small scale of the layer thickness relative to the large scale of the overall spiral structure, reveals the bulk of the spiral has an unexpected simple behaviour while there are boundary layers in a surface region near the inner and outer windings. There are further finer-structure boundary layers at the very beginning and very end of the spiral. In all these regions analytical solutions are found providing simple expressions for the deformations and in particular the tension in the inextensible layer. Comparisons are shown between these expressions and detailed finite-element solutions of the problem. These reduced-order models provide a simple way of accounting for stresses induced by expansion of the spiral structure.

Keywords: Asymptotic analysis, homogenisation, linear elasticity

PhySH: composite materials

2000 MSC: 35B27, 74B05

*Corresponding author

Email addresses: `timms@maths.ox.ac.uk` (Robert Timms), `steven.psaltis@qut.edu.au` (Steven Psaltis), `please@maths.ox.ac.uk` (Colin P. Please), `chapman@maths.ox.ac.uk` (S. Jon Chapman)

1. Introduction

In this paper we develop a reduced-order model to explain the stress distribution created by isotropic expansion in spirally-wound layered materials containing a reinforcing inextensible sheet and linearly elastic matrix layer. Our initial motivation lies in the need for greater understanding of the stress and strain distributions within cylindrical batteries, which have a spiral structure similar to that considered here. Our asymptotic methodology is guided by recent work that systematically studied the electrical and thermal behaviour of such spirally-wound devices [1].

There is considerable interest in understanding the mechanical deformations that occur in a lithium-ion battery because their long-term degradation is known to strongly depend on the pressure applied to the cell during manufacturing and operation [2]. Stresses in the battery tend to be considered at either a very small scale (~ 10 microns, the size of the particles that make up the electrodes in the battery) or at a macroscale (~ 1 cm, the size of the battery). The stresses are primarily created by expansion of the active material particles due to changes in state of lithiation or by expansion of all battery materials due to changes in temperature. Here we shall concentrate on the macroscopic stresses. Since the stress affects the electrochemical behaviour in the battery, there is strong coupling between electrochemistry, thermal effects and mechanical deformation. The stresses can also cause direct degradation of the battery by causing buckling and delamination. Such behaviour has been observed in cylindrical cells using CT scans over the cell lifetime, and is often localised near the centre of the cell in the inner few windings of the spirally-wound battery [3, 4, 5, 6, 7]; it is clearly seen in Figure 4 of [8].

In this paper we consider an idealised structure that is similar to a battery but sufficiently simple to make analytical progress. We assume that the spiral is tall so that we can consider generalised plane strain and examine deformations in a cross-sectional plane. The main analysis exploits the fact that the spiral has many windings and hence the thickness of the repeating layers is small compared to the size of the battery. We take the spiral to be made of a matrix of elastic material (the active battery material) and a reinforcing inextensible material (the current collectors of the battery). Although the problem is motivated by battery behaviour the analysis is of general interest to any layered spirally-wound elastic material where one layer is sufficiently stiff to be taken as inextensible.

In Section 2 we formulate the model. We treat the simplest case in which the matrix response is linearly elastic, the system is in generalised plane strain, and the expansion of the material is prescribed. We make a further simplification that the reinforcing sheet can be treated as an infinitesimally thin, inextensible inclusion with no bending moment. Both the matrix and the reinforcing sheet expand in a prescribed isotropic manner. In Section 3 we use asymptotic methods, exploiting the ratio of the thickness of the matrix layer to the size of the spiral. The analysis reveals that the solution consists of an “outer region” throughout the bulk of the domain in which the radial and hoop stresses take a simple form, but in which there is no shear stress. Away from the outer region, near the inner and outer surfaces, boundary layers occur in which the stresses vary dramatically. We also show there

are additional boundary layers near the beginning and end of the winds of the spiral. The analysis results in simple closed form expressions for the stresses and strains in the matrix, and tension in the reinforcing sheet, thus revealing how the material properties and local expansion affect the macroscale stress. To demonstrate the efficacy of the solution approach, comparisons between our asymptotic solution and numerical results obtained from solving the governing equations with the detailed geometry using COMSOL [9] are provided in Section 4. Finally, in Section 5 we summarise the findings.

2. Model Formulation

In this section we develop a model for the mechanical response of a spirally-wound layered material subject to some prescribed isotropic expansion/contraction. The later analysis will be carried out using a nondimensional formulation so, in the following, we use a superscript star to represent a dimensional quantity.

2.1. Geometry

We consider deformations that occur in tall samples of spirally-wound layered materials, with a cross-section as illustrated in Figure 1 (b). A single reinforcing sheet of metal has been partially covered on one side by a material (the matrix), as shown in Figure 1 (a), whose properties may vary with distance through the layer. The reinforcing sheet and matrix are then rolled into a spiral to produce the structure illustrated in Figure 1 (b), where the reinforcing sheet wraps around so that both the inner and outer surface are covered with this material. Our interest is to determine the stresses and displacements that occur within the structure when the matrix and/or reinforcing sheet undergo some prescribed isotropic expansion. To make analytical progress, we shall concentrate on the behaviour in any cross-section and not consider behaviour near the top or bottom of the tall spiral.

We assume that the matrix has uniform thickness h^* and that the reinforcing sheet is infinitesimally thin. We take the inner radius of the domain to be L_0^* , and the outer radius to be L^* (measured at $\theta = 0$). We assume the material is rolled as an Archimedean spiral, as shown in Figure 1 (b), so that the reinforcing sheet is given by $r^* = L_0^* + h^*\theta/2\pi$ in polar coordinates. To account for a possible multiple-layer structure of the matrix we allow the material properties to vary with distance through the layer, i.e. they may depend on $r^* - h^*\theta/2\pi$.

We denote the entire domain of the spiral as Ω and the region occupied by the matrix as Ω_m . The boundary between neighbouring regions of matrix represents the reinforcing sheet, and is denoted by Γ . Finally, the inner and outer boundaries of the spiral are denoted by Γ_{in} and Γ_{out} .

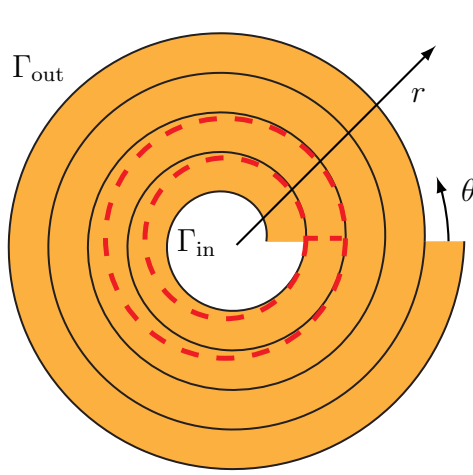
2.2. Physics

2.2.1. The matrix

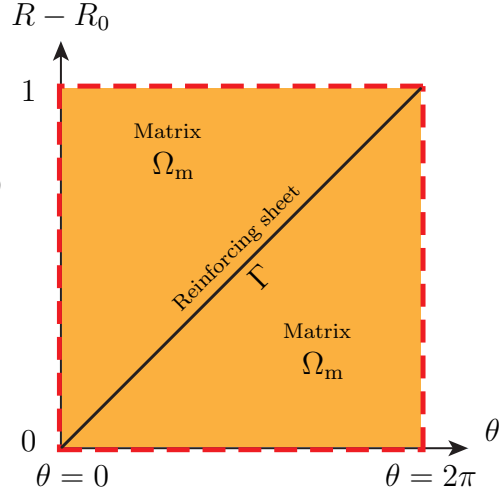
We assume that the strains are small enough that within the matrix we may use linear elasticity theory, and that the material is isotropic. The elastic strain tensor,



(a) Unrolled strip showing sections of coated and uncoated reinforcing sheet.



(b) Spiral geometry.



(c) Periodic unit cell in polar coordinates.

Figure 1: Representation of Archimedean spiral geometry. (a) the unrolled reinforcing sheet as a solid black line, partially coated with matrix. (b) the spiral geometry, where the red dashed circles show the boundaries of a representative periodic cell. (c) the representative periodic cell in polar coordinates, given in $R - R_0 = r/\delta$ and θ , where R_0 is the integer part of R .

$\boldsymbol{\varepsilon}_e^*$, is written as

$$\boldsymbol{\varepsilon}_e^* = \boldsymbol{\varepsilon}^* - \alpha^* \mathbf{1} = \frac{1}{2} (\nabla^* \mathbf{u}^* + (\nabla^* \mathbf{u}^*)^T) - \alpha^* \mathbf{1} \quad \text{in } \Omega_m, \quad (1)$$

where $\boldsymbol{\varepsilon}^*$ is the total strain, \mathbf{u}^* is the displacement, and $\mathbf{1}$ is the identity tensor. Here $\alpha^* = \alpha^*(\mathbf{x}^*)$ describes the spatially-dependent isotropic material expansion of the matrix, where \mathbf{x}^* is the spatial coordinate. The expansion is taken to be prescribed, and could be due to either thermal expansion or swelling (such as during lithiation in a battery), for example. Note that α^* is the *linear* expansion coefficient which is approximately three times smaller than the *volumetric* expansion coefficient for isotropic materials.

The stress is related to the strain via Hooke's law

$$\boldsymbol{\sigma}^* = \mathbb{C}^* : \boldsymbol{\varepsilon}_e^* \quad \text{in } \Omega_m, \quad (2)$$

where $\boldsymbol{\sigma}^*$ is the stress tensor and \mathbb{C}^* is the stiffness tensor of the matrix. In general the stiffness tensor is a function of space so that $\mathbb{C}^* = \mathbb{C}^*(\mathbf{x}^*)$. For an isotropic material we have, in suffix notation,

$$\sigma_{ij} = \lambda^* \delta_{ij} \varepsilon_{kk}^* + \mu^* \left(\frac{\partial u_i^*}{\partial x_j^*} + \frac{\partial u_j^*}{\partial x_i^*} \right) - \alpha^* (3\lambda^* + 2\mu^*) \delta_{ij} \quad \text{in } \Omega_m, \quad (3)$$

where $\lambda^* = \lambda^*(\mathbf{x}^*)$ is the first Lamé parameter, $\mu^* = \mu^*(\mathbf{x}^*)$ is the second Lamé parameter (or shear modulus), and δ_{ij} is the Kronecker delta. We assume the system is in mechanical equilibrium, so that

$$\nabla^* \cdot \boldsymbol{\sigma}^* = 0 \quad \text{in } \Omega_m. \quad (4)$$

We will focus on the case of a cylindrical geometry under conditions of generalised plane strain, so that the displacement is given by $\mathbf{u}^* = (u^*, v^*, \varepsilon_{zz}^{0*} z^*)$, where ε_{zz}^{0*} is the constant axial strain. Adopting cylindrical polar coordinates, the non-zero components of the total strain tensor are

$$\begin{aligned} \varepsilon_{rr}^* &= \frac{\partial u^*}{\partial r^*}, & \varepsilon_{\theta\theta}^* &= \frac{1}{r^*} \left(\frac{\partial v^*}{\partial \theta} + u^* \right), \\ \varepsilon_{r\theta}^* &= \frac{1}{2} \left(\frac{1}{r^*} \frac{\partial u^*}{\partial \theta} + \frac{\partial v^*}{\partial r^*} - \frac{v^*}{r^*} \right), & \varepsilon_{zz}^* &= \varepsilon_{zz}^{0*}, \end{aligned} \quad \text{in } \Omega_m. \quad (5)$$

The corresponding components of the stress tensor are

$$\sigma_{rr}^* = (\lambda^* + 2\mu^*) \varepsilon_{rr}^* + \lambda^* (\varepsilon_{\theta\theta}^* + \varepsilon_{zz}^{0*}) - \alpha^* (3\lambda^* + 2\mu^*) \quad \text{in } \Omega_m, \quad (6)$$

$$\sigma_{\theta\theta}^* = \lambda^* (\varepsilon_{rr}^* + \varepsilon_{zz}^{0*}) + (\lambda^* + 2\mu^*) \varepsilon_{\theta\theta}^* - \alpha^* (3\lambda^* + 2\mu^*) \quad \text{in } \Omega_m, \quad (7)$$

$$\sigma_{r\theta}^* = 2\mu^* \varepsilon_{r\theta}^* \quad \text{in } \Omega_m, \quad (8)$$

where α^* , μ^* and λ^* may in general be functions of space.

2.2.2. Reinforcing sheet

In order to make analytical progress we will assume that the reinforcing sheet is infinitesimally thin and inextensible, with zero bending stiffness. However, in order to account for expansion of the reinforcing sheet, we do allow its natural length to change due to a prescribed, constant, isotropic expansion α_s^* , where again α_s^* represents the linear expansion coefficient. Thus, we model the reinforcing sheet as an inextensible (after the prescribed expansion) inclusion which can support a tension along its length.

The inextensibility condition implies that on the curve Γ we must preserve arc length. However, this arc length may change in response to the prescribed expansion α_s^* . Here we derive the inextensibility condition in cylindrical coordinates. We parameterise the surface generated by taking the original position of the boundary Γ extended in the perpendicular plane with s^* and t^* as $(r^*, \theta, z^*) = (r_0^*(s^*), \theta_0(s^*), t^*)$. Here s^* is the arc length along Γ in the cross-sectional plane and t^* is the out of plane distance. Consider the deformation of a small line segment joining two particles whose polar coordinates are (r^*, θ, z^*) and $(r^* + \delta r^*, \theta + \delta \theta, z^* + \delta z^*)$. The vector joining the two particles is given to leading order by

$$\delta \mathbf{X}^* \sim \delta r^* \mathbf{e}_r + r^* \delta \theta \mathbf{e}_\theta + \delta z^* \mathbf{e}_z. \quad (9)$$

With the assumption of generalised plane strain the displacement field takes the form $\mathbf{u}^* = u^*(r^*, \theta) \mathbf{e}_r + v^*(r^*, \theta) \mathbf{e}_\theta + \varepsilon_{zz}^{0*} z^* \mathbf{e}_z$, so that the line element $\delta \mathbf{X}^*$ is displaced to

$$\delta \mathbf{x}^* = \delta \mathbf{X}^* + \left(\frac{\partial u^*}{\partial r^*} \delta r^* + \frac{\partial u^*}{\partial \theta} \delta \theta - v^* \delta \theta \right) \mathbf{e}_r + \left(\frac{\partial v^*}{\partial r^*} \delta r^* + \frac{\partial v^*}{\partial \theta} \delta \theta + u^* \delta \theta \right) \mathbf{e}_\theta + \varepsilon_{zz}^{0*} \delta z^* \mathbf{e}_z, \quad (10)$$

giving

$$|\delta \mathbf{x}^*|^2 = |\delta \mathbf{X}^*|^2 + (\delta r^* \quad r^* \delta \theta \quad \delta z^*) \begin{pmatrix} \varepsilon_{rr}^* & \varepsilon_{r\theta}^* & 0 \\ \varepsilon_{r\theta}^* & \varepsilon_{\theta\theta}^* & *0 \\ 0 & 0 & \varepsilon_{zz}^{0*} \end{pmatrix} \begin{pmatrix} \delta r^* \\ r^* \delta \theta \\ \delta z^* \end{pmatrix}. \quad (11)$$

The inextensibility condition requires that the new length is equal to the length of the original line element after it undergoes an isotropic expansion, i.e. we require

$$|\delta \mathbf{x}^*|^2 = |\delta \mathbf{X}^*|^2 + (\delta r^* \quad r^* \delta \theta \quad \delta z^*) \begin{pmatrix} \alpha_s^* & 0 & 0 \\ 0 & \alpha_s^* & 0 \\ 0 & 0 & \alpha_s^* \end{pmatrix} \begin{pmatrix} \delta r^* \\ r^* \delta \theta \\ \delta z^* \end{pmatrix}. \quad (12)$$

Subtracting (12) from (11), and considering line segments $\delta \mathbf{X}^*$ in the plane (variations with s^*) and perpendicular to the plane (variations with t^*) gives us two conditions. These are

$$(\dot{r}_0^* \quad r_0^* \dot{\theta}_0 \quad 0) \begin{pmatrix} \varepsilon_{rr}^* - \alpha_s^* & \varepsilon_{r\theta}^* & 0 \\ \varepsilon_{r\theta}^* & \varepsilon_{\theta\theta}^* - \alpha_s^* & 0 \\ 0 & 0 & \varepsilon_{zz}^{0*} - \alpha_s^* \end{pmatrix} \begin{pmatrix} \dot{r}_0^* \\ r_0^* \dot{\theta}_0 \\ 0 \end{pmatrix} = 0 \quad \text{on } \Gamma, \quad (13)$$

where the dot represents a derivative with respect to arc length of the original curve

s^* , and

$$(0 \ 0 \ 1) \begin{pmatrix} \varepsilon_{rr}^* - \alpha_s^* & \varepsilon_{r\theta}^* & 0 \\ \varepsilon_{r\theta}^* & \varepsilon_{\theta\theta}^* - \alpha_s^* & 0 \\ 0 & 0 & \varepsilon_{zz}^{0*} - \alpha_s^* \end{pmatrix} \begin{pmatrix} 0 \\ 0 \\ 1 \end{pmatrix} = 0 \quad \text{on } \Gamma, \quad (14)$$

respectively. Crucially (14) shows that the entire spiral grows axially by the expansion factor of the reinforcing layer, and we therefore need

$$\varepsilon_{zz}^{0*} = \alpha_s^*. \quad (15)$$

For simplicity in subsequent analysis, we will refer to (13) as the inextensibility condition.

The inextensible reinforcing sheet will develop a tension in the cross-sectional plane due to the jump in tangential stress across the interface, given by

$$\frac{\partial T^*}{\partial s^*} = [\mathbf{t} \cdot \boldsymbol{\sigma}^* \mathbf{n}]_-^+ \quad \text{on } \Gamma, \quad (16)$$

where T^* is the tension in the cross-sectional plane on the curve Γ , $[\cdot]_-^+$ represents the jump in the enclosed quantity across Γ , and \mathbf{n} and \mathbf{t} are the unit normal and unit tangent vector (in the plane) to Γ , respectively. The tension in the curved reinforcing sheet creates a jump in the normal stress given by

$$T^* \kappa^* = [\mathbf{n} \cdot \boldsymbol{\sigma}^* \mathbf{n}]_-^+ \quad \text{on } \Gamma, \quad (17)$$

where κ^* is the curvature of Γ . Finally, the displacement must be continuous across the reinforcing sheet, so that

$$[\mathbf{u}^*]_-^+ = \mathbf{0} \quad \text{on } \Gamma. \quad (18)$$

2.2.3. Boundary conditions

We assume that both the inner and outer surfaces of the spiral are stress-free, so that

$$\boldsymbol{\sigma}^* \mathbf{n} = \mathbf{0} \quad \text{on } \Gamma_{\text{in}} \text{ and } \Gamma_{\text{out}}. \quad (19)$$

2.3. Nondimensionalisation

We use the outer radius of the domain L^* as our length scale. The spatial coordinate \mathbf{x}^* , displacement \mathbf{u}^* , strain tensor $\boldsymbol{\varepsilon}^*$, stress tensor $\boldsymbol{\sigma}^*$, and tension T^* are nondimensionalised by setting

$$\mathbf{x}^* = L^* \mathbf{x}, \quad \mathbf{u}^* = L^* \alpha_{\text{typ}}^* \mathbf{u}, \quad \boldsymbol{\varepsilon}^* = \alpha_{\text{typ}}^* \boldsymbol{\varepsilon}, \quad \boldsymbol{\sigma}^* = \mu_{\text{typ}}^* \alpha_{\text{typ}}^* \boldsymbol{\sigma}, \quad T^* = \mu_{\text{typ}}^* \alpha_{\text{typ}}^* L^* T, \quad (20)$$

where α_{typ}^* and μ_{typ}^* are typical values of the expansion coefficient and shear modulus chosen to be representative of the constituent materials of the matrix.

The reinforcing sheet is now given by $r = r_0 + \delta\theta/2\pi$ where $r_0 = L_0^*/L^*$ and $\delta = h^*/L^*$. The parameter δ is critical to our analysis as it represents the ratio of

the thickness of the matrix to the radius of the domain, and will be assumed to be small. This limit can also be interpreted as the spiral having many windings. The equilibrium equation (4) becomes

$$\nabla \cdot \boldsymbol{\sigma} = 0 \quad \text{in } \Omega_m, \quad (21)$$

with

$$\sigma_{ij} = \lambda \delta_{ij} \varepsilon_{kk} + \mu \left(\frac{\partial u_i}{\partial x_j} + \frac{\partial u_j}{\partial x_i} \right) - \alpha (3\lambda + 2\mu) \delta_{ij} \quad \text{in } \Omega_m, \quad (22)$$

where the dimensionless coefficients are given by

$$\lambda(\mathbf{x}) = \lambda^*(\mathbf{x}^*)/\mu_{\text{typ}}^*, \quad \mu(\mathbf{x}) = \mu^*(\mathbf{x}^*)/\mu_{\text{typ}}^*, \quad \alpha(\mathbf{x}) = \alpha^*(\mathbf{x}^*)/\alpha_{\text{typ}}^*. \quad (23)$$

The jump conditions at the interface become

$$\frac{\partial T}{\partial s} = [\mathbf{t} \cdot \boldsymbol{\sigma} \mathbf{n}]_-^+ \quad \text{on } \Gamma, \quad (24)$$

$$T\kappa = [\mathbf{n} \cdot \boldsymbol{\sigma} \mathbf{n}]_-^+ \quad \text{on } \Gamma, \quad (25)$$

$$[\mathbf{u}]_-^+ = \mathbf{0} \quad \text{on } \Gamma, \quad (26)$$

where $\kappa = L^* \kappa^*$. Since the interface Γ is given by the equation

$$f(r, \theta) = r - \frac{\delta \theta}{2\pi} = \text{constant}, \quad (27)$$

we have

$$\begin{aligned} \mathbf{n} &= \frac{\nabla f}{|\nabla f|} = \left(\frac{\partial f}{\partial r} \mathbf{e}_r + \frac{1}{r} \frac{\partial f}{\partial \theta} \mathbf{e}_\theta \right) \left(\left(\frac{\partial f}{\partial r} \right)^2 + \frac{1}{r^2} \left(\frac{\partial f}{\partial \theta} \right)^2 \right)^{-1/2} \\ &= \left(1 + \frac{\delta^2}{4\pi^2 r^2} \right)^{-1/2} \begin{pmatrix} 1 \\ -\frac{\delta}{2\pi r} \end{pmatrix}, \end{aligned} \quad (28)$$

and

$$\mathbf{t} = \left(1 + \frac{\delta^2}{4\pi^2 r^2} \right)^{-1/2} \begin{pmatrix} -\frac{\delta}{2\pi r} \\ -1 \end{pmatrix}. \quad (29)$$

In order for the Archimedean spiral to be inextensible we require that the strain satisfies the dimensionless version of (13). Introducing τ to parameterise the spiral by using $r = \tau$, $\theta = 2\pi\tau/\delta$, and differentiating the position vector $\mathbf{x} = r\mathbf{e}_r$ gives

$$\frac{\partial \mathbf{x}}{\partial \tau} = \mathbf{e}_r \frac{\partial r}{\partial \tau} + r \frac{\partial \mathbf{e}_r}{\partial \theta} \frac{\partial \theta}{\partial \tau} = \mathbf{e}_r + \frac{2\pi r}{\delta} \mathbf{e}_\theta = \frac{\partial \mathbf{x}}{\partial s} \frac{\partial s}{\partial \tau}. \quad (30)$$

Thus we find that

$$\frac{\partial s}{\partial \tau} = \left(1 + \frac{4\pi^2 r^2}{\delta^2} \right)^{1/2}. \quad (31)$$

It then follows that

$$\frac{\partial r}{\partial s} = \frac{\partial r}{\partial \tau} \frac{\partial \tau}{\partial s} = \left(1 + \frac{4\pi^2 r^2}{\delta^2}\right)^{-1/2} \quad \text{and} \quad r \frac{\partial \theta}{\partial s} = r \frac{\partial \theta}{\partial \tau} \frac{\partial \tau}{\partial s} = \frac{2\pi r}{\delta} \left(1 + \frac{4\pi^2 r^2}{\delta^2}\right)^{-1/2}, \quad (32)$$

so that the inextensibility conditions (13) and (14) read

$$\frac{\delta^2}{(2\pi r)^2} (\varepsilon_{rr} - \alpha_s) + \frac{2\delta}{2\pi r} \varepsilon_{r\theta} + \varepsilon_{\theta\theta} - \alpha_s = 0, \quad \text{and} \quad \varepsilon_{zz} = \alpha_s \quad \text{on } \Gamma, \quad (33)$$

where $\alpha_s = \alpha_s^*/\alpha_{\text{typ}}^*$. Finally, the boundary conditions are

$$\boldsymbol{\sigma} \mathbf{n} = \mathbf{0} \quad \text{on } \Gamma_{\text{in}} \text{ and } \Gamma_{\text{out}}. \quad (34)$$

3. Asymptotic analysis

In this section we consider the behaviour of the model in the limit $\delta \ll 1$, which corresponds to the case of the spiral containing many winds. In our analysis, we will assume that all other parameters in the model are $\mathcal{O}(1)$. This is true for practical battery materials with two exceptions: i) the electrodes in a cell are kept apart electrically by a separator which is typically much weaker than other components, hence its dimensionless elastic moduli will be small, and ii) the expansion due to thermal effects is typically much smaller than that due to lithiation. The analysis presented here is still relevant to real cells, but further simplifications might be made by exploiting these small parameters. We will exploit the methods of multiple-scales homogenisation and boundary layer analysis ([10, 11]) to derive a simplified model. We will demonstrate that in the bulk of the material the strains vary smoothly and can be found readily – we refer to this as the “bulk region” of the problem and it corresponds to the “outer region” of an asymptotic solution. However, there is a narrow region that begins near the inner surface and extends a few winds into the bulk where the strains change rapidly – we refer to this as the “surface region” and it corresponds to a “boundary layer in r ”. We also consider a small region close to the very end of the winding which is a few layers thick and only a small angle in extent. We refer to this as the “end-of-winding region” and it corresponds to a “boundary layer in r and θ ”. There will also be a similar boundary layer structure near the outer surface of the spiral, but we will not present the analysis here. This general structure of the solution is shown in Figure 2.

3.1. Homogenisation in the bulk region

We start by considering the behaviour in the bulk region where r and θ are $\mathcal{O}(1)$. We exploit the method of multiple-scales homogenisation, writing the problem so that the solution depends on both macroscale and microscale variables [10]. Crucially our geometry is periodic in polar coordinates: increasing θ by 2π is equivalent to increasing r by δ . This enables us to impose periodicity on the microscale in the usual way. The periodically repeated unit cell in cylindrical coordinates corresponds

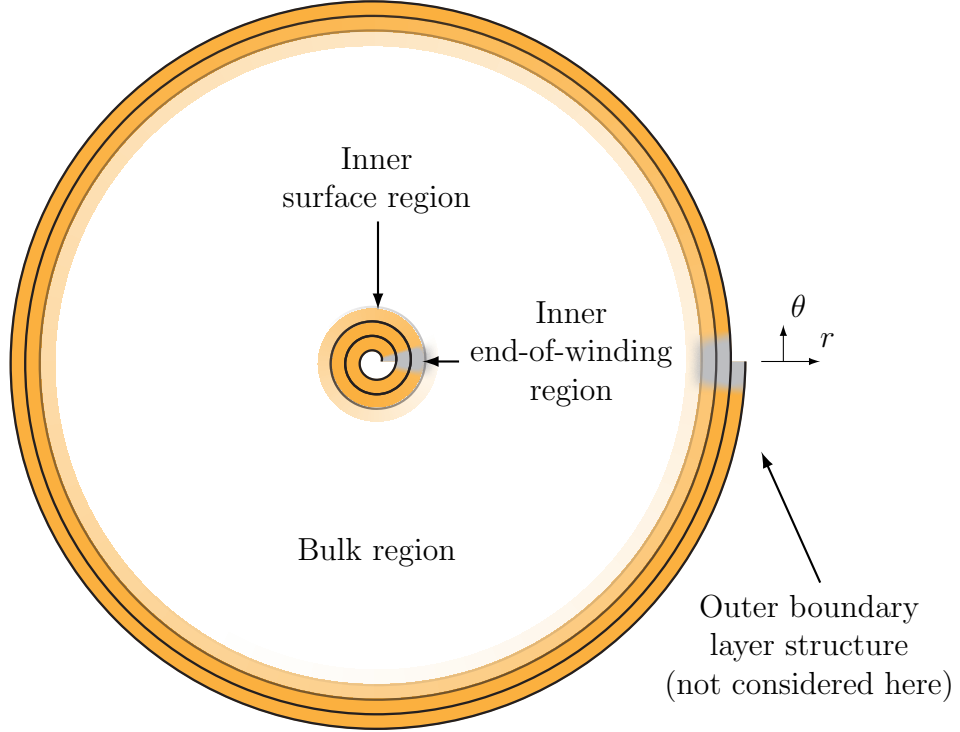


Figure 2: Overall boundary layer structure of solution.

to an annular region bounded by concentric circles, as indicated in Figure 1 (b). Introducing the microscale variable in the radial direction, $R = r/\delta$, we can illustrate the unit cell in the (R, θ) plane, as shown in Figure 1 (c). We treat R and r as independent variables, eliminating the degeneracy that this introduces by requiring that the solution is exactly periodic in R with unit period.

Since the matrix is of a layered form we know that the material properties α , λ and μ will depend on the short scale $R - \theta/2\pi$. Furthermore we restrict ourselves to the case where the only short scale variations arise due to this uniform layered structure. In practice there are macroscale variations in expansion and we account for this by allowing the expansion coefficient in the matrix to depend on the long scale r . Hence the functional forms of the material properties are $\alpha = \alpha(r, R - \theta/2\pi)$, $\lambda = \lambda(R - \theta/2\pi)$, and $\mu = \mu(R - \theta/2\pi)$ all of which are periodic in $R - \theta/2\pi$ with period 1. This assumed functional form implies that our homogenised problem will be a function of the macroscale radial coordinate r only.

In multiple scales form equations (21)–(26) become

$$\varepsilon_{rr} = \frac{1}{\delta} \frac{\partial u}{\partial R} + \frac{\partial u}{\partial r}, \quad (35a)$$

$$\varepsilon_{\theta\theta} = \frac{1}{r} \left(\frac{\partial v}{\partial \theta} + u \right), \quad (35b)$$

$$\varepsilon_{r\theta} = \frac{1}{2} \left(\frac{1}{r} \frac{\partial u}{\partial \theta} + \frac{1}{\delta} \frac{\partial v}{\partial R} + \frac{\partial v}{\partial r} - \frac{v}{r} \right), \quad (35c)$$

$$\sigma_{rr} = (\lambda + 2\mu)\varepsilon_{rr} + \lambda\varepsilon_{\theta\theta} + \lambda\alpha_s - \alpha(3\lambda + 2\mu), \quad (35d)$$

$$\sigma_{\theta\theta} = \lambda\varepsilon_{rr} + (\lambda + 2\mu)\varepsilon_{\theta\theta} + \lambda\alpha_s - \alpha(3\lambda + 2\mu), \quad (35e)$$

$$\sigma_{r\theta} = 2\mu\varepsilon_{r\theta}, \quad (35f)$$

$$0 = \frac{1}{r} \left(\frac{\partial}{\partial r} + \frac{1}{\delta} \frac{\partial}{\partial R} \right) (r\sigma_{rr}) + \frac{1}{r} \frac{\partial\sigma_{r\theta}}{\partial\theta} - \frac{\sigma_{\theta\theta}}{r}, \quad (35g)$$

$$0 = \frac{1}{r} \left(\frac{\partial}{\partial r} + \frac{1}{\delta} \frac{\partial}{\partial R} \right) (r\sigma_{r\theta}) + \frac{1}{r} \frac{\partial\sigma_{\theta\theta}}{\partial\theta} + \frac{\sigma_{r\theta}}{r}, \quad (35h)$$

$$0 = \frac{\delta^2}{(2\pi r)^2} (\varepsilon_{rr} - \alpha_s) + \frac{2\delta}{2\pi r} \varepsilon_{r\theta} + \varepsilon_{\theta\theta} - \alpha_s \quad \text{on } R = R_0 + \theta/2\pi, \quad (35i)$$

$$\left(1 + \frac{4\pi^2 r^2}{\delta^2}\right)^{-1/2} \frac{2\pi}{\delta} \frac{\partial T}{\partial\theta} = \left(1 + \frac{\delta^2}{4\pi^2 r^2}\right)^{-1} \left[-(\delta/2\pi r \quad 1) \begin{pmatrix} \sigma_{rr} & \sigma_{r\theta} \\ \sigma_{r\theta} & \sigma_{\theta\theta} \end{pmatrix} \begin{pmatrix} 1 \\ -\delta/2\pi r \end{pmatrix} \right]_{-}^{+} \quad (35j)$$

on $R = R_0 + \theta/2\pi$,

$$\left(\frac{1}{r} + \frac{\delta^2}{8\pi^2 r^3} + \dots\right) T = \left[(1 \quad -\delta/2\pi r) \begin{pmatrix} \sigma_{rr} & \sigma_{r\theta} \\ \sigma_{r\theta} & \sigma_{\theta\theta} \end{pmatrix} \begin{pmatrix} 1 \\ -\delta/2\pi r \end{pmatrix} \right]_{-}^{+} \quad (35k)$$

on $R = R_0 + \theta/2\pi$,

$$[u]_{-}^{+} = 0 \text{ on } R = R_0 + \theta/2\pi, \quad (35l)$$

$$[v]_{-}^{+} = 0 \text{ on } R = R_0 + \theta/2\pi. \quad (35m)$$

Expanding each component of the solution in powers of δ in the form

$$u \sim u^{(0)} + \delta u^{(1)} + \dots, \quad (36)$$

we find, at leading order in δ , the problem becomes

$$0 = \frac{\partial u^{(0)}}{\partial R}, \quad (37a)$$

$$\varepsilon_{\theta\theta}^{(0)} = \frac{1}{r} \left(\frac{\partial v^{(0)}}{\partial\theta} + u^{(0)} \right), \quad (37b)$$

$$0 = \frac{\partial v^{(0)}}{\partial R}, \quad (37c)$$

$$\sigma_{rr}^{(0)} = (\lambda + 2\mu)\varepsilon_{rr}^{(0)} + \lambda\varepsilon_{\theta\theta}^{(0)} + \lambda\alpha_s - \alpha(3\lambda + 2\mu), \quad (37d)$$

$$\sigma_{\theta\theta}^{(0)} = \lambda\varepsilon_{rr}^{(0)} + (\lambda + 2\mu)\varepsilon_{\theta\theta}^{(0)} + \lambda\alpha_s - \alpha(3\lambda + 2\mu), \quad (37e)$$

$$\sigma_{r\theta}^{(0)} = 2\mu\varepsilon_{r\theta}^{(0)}, \quad (37f)$$

$$0 = \frac{\partial\sigma_{rr}^{(0)}}{\partial R}, \quad (37g)$$

$$0 = \frac{\partial\sigma_{r\theta}^{(0)}}{\partial R}, \quad (37h)$$

$$0 = \varepsilon_{\theta\theta}^{(0)} - \alpha_s \text{ on } R = R_0 + \theta/2\pi, \quad (37i)$$

$$\frac{1}{r} \frac{\partial T^{(0)}}{\partial \theta} = - \left[\sigma_{r\theta}^{(0)} \right]_{-}^{+} \text{ on } R = R_0 + \theta/2\pi, \quad (37j)$$

$$\frac{1}{r} T^{(0)} = \left[\sigma_{rr}^{(0)} \right]_{-}^{+} \text{ on } R = R_0 + \theta/2\pi, \quad (37k)$$

$$\left[u^{(0)} \right]_{-}^{+} = \left[v^{(0)} \right]_{-}^{+} = 0 \text{ on } R = R_0 + \theta/2\pi. \quad (37l)$$

From (37a), (37c), (37g), and (37h) we immediately conclude that the displacements, $u^{(0)}$ and $v^{(0)}$, and normal and shear stresses, $\sigma_{rr}^{(0)}$ and $\sigma_{r\theta}^{(0)}$, are all independent of R . Thus, periodicity implies, from (37j) and (37k), that the jump in normal and shear stress across the inclusion $R = R_0 + \theta/2\pi$ is zero, and it follows that the tension is zero to leading order. The inextensibility condition (37a) gives $\varepsilon_{\theta\theta}^{(0)} = \alpha_s$ on $R = \theta/2\pi$, but since the leading order displacements do not depend on R then, by (37b), neither does the leading order azimuthal strain. Thus $\varepsilon_{\theta\theta}^{(0)} = \alpha_s$ everywhere.

At the next order in δ we find

$$\varepsilon_{rr}^{(0)} = \frac{\partial u^{(0)}}{\partial r} + \frac{\partial u^{(1)}}{\partial R}, \quad (38a)$$

$$\varepsilon_{\theta\theta}^{(1)} = \frac{1}{r} \left(\frac{\partial v^{(1)}}{\partial \theta} + u^{(1)} \right), \quad (38b)$$

$$\varepsilon_{r\theta}^{(0)} = \frac{1}{2} \left(\frac{1}{r} \frac{\partial u^{(0)}}{\partial \theta} + \frac{\partial v^{(0)}}{\partial r} - \frac{v^{(0)}}{r} + \frac{\partial v^{(1)}}{\partial R} \right), \quad (38c)$$

$$\sigma_{rr}^{(1)} = (\lambda + 2\mu) \varepsilon_{rr}^{(1)} + \lambda \varepsilon_{\theta\theta}^{(1)}, \quad (38d)$$

$$\sigma_{\theta\theta}^{(1)} = \lambda \varepsilon_{rr}^{(1)} + (\lambda + 2\mu) \varepsilon_{\theta\theta}^{(1)}, \quad (38e)$$

$$\sigma_{r\theta}^{(1)} = 2\mu \varepsilon_{r\theta}^{(1)}, \quad (38f)$$

$$-r \frac{\partial \sigma_{rr}^{(1)}}{\partial R} = \frac{\partial (r \sigma_{rr}^{(0)})}{\partial r} + \frac{\partial \sigma_{r\theta}^{(0)}}{\partial \theta} - \sigma_{\theta\theta}^{(0)} \equiv F(r, R, \theta), \quad (38g)$$

$$-r \frac{\partial \sigma_{r\theta}^{(1)}}{\partial R} = \frac{\partial (r \sigma_{r\theta}^{(0)})}{\partial r} + \frac{\partial \sigma_{\theta\theta}^{(0)}}{\partial \theta} + \sigma_{r\theta}^{(0)} \equiv G(r, R, \theta), \quad (38h)$$

$$0 = \varepsilon_{\theta\theta}^{(1)} + \frac{1}{\pi r} \varepsilon_{r\theta}^{(0)} \text{ on } R = R_0 + \theta/2\pi, \quad (38i)$$

$$\frac{1}{r} \frac{\partial T^{(1)}}{\partial \theta} = - \left[\sigma_{r\theta}^{(1)} - \frac{\sigma_{\theta\theta}^{(0)}}{2\pi r} \right]_{-}^{+} \text{ on } R = R_0 + \theta/2\pi, \quad (38j)$$

$$\frac{1}{r} T^{(1)} = \left[\sigma_{rr}^{(1)} \right]_{-}^{+} \text{ on } R = R_0 + \theta/2\pi, \quad (38k)$$

$$\left[u^{(1)} \right]_{-}^{+} = \left[v^{(1)} \right]_{-}^{+} = 0 \text{ on } R = R_0 + \theta/2\pi. \quad (38l)$$

Now, the leading order stresses can be written as

$$\sigma_{rr}^{(0)} = (\lambda + 2\mu) \left(\frac{\partial u^{(0)}}{\partial r} + \frac{\partial u^{(1)}}{\partial R} \right) + 2\lambda \alpha_s - \alpha(3\lambda + 2\mu), \quad (39)$$

$$\sigma_{\theta\theta}^{(0)} = \frac{\lambda}{\lambda + 2\mu} \sigma_{rr}^{(0)} + \frac{2\mu(\alpha_s - \alpha)(3\lambda + 2\mu)}{\lambda + 2\mu}, \quad (40)$$

$$\sigma_{r\theta}^{(0)} = \mu \left(\frac{1}{r} \frac{\partial u^{(0)}}{\partial \theta} + \frac{\partial v^{(0)}}{\partial r} - \frac{v^{(0)}}{r} + \frac{\partial v^{(1)}}{\partial R} \right), \quad (41)$$

with $u^{(1)}$ and $v^{(1)}$ periodic, with period 1 in R and period 2π in θ . Since $u^{(1)}$ is periodic in R with period 1 then

$$\int_0^1 \frac{\partial u^{(1)}}{\partial R} dR = 0, \quad (42)$$

and thus it follows from (39) that

$$\begin{aligned} 0 &= \int_0^1 \frac{\partial u^{(1)}}{\partial R} dR \\ &= -\frac{\partial u^{(0)}}{\partial r} + \sigma_{rr}^{(0)} \int_0^1 \frac{1}{\lambda + 2\mu} dR - 2\alpha_s \int_0^1 \frac{\lambda}{\lambda + 2\mu} dR + \int_0^1 \frac{\alpha(3\lambda + 2\mu)}{(\lambda + 2\mu)} dR. \end{aligned} \quad (43)$$

Similarly, we can use the periodicity in $v^{(1)}$, along with (41), to show that

$$0 = \int_0^1 \frac{\partial v^{(1)}}{\partial R} dR = -\left(\frac{1}{r} \frac{\partial u^{(0)}}{\partial \theta} + \frac{\partial v^{(0)}}{\partial r} - \frac{v^{(0)}}{r} \right) + \sigma_{r\theta}^{(0)} \int_0^1 \frac{1}{\mu} dR. \quad (44)$$

We can integrate over R in the first order momentum balances (38g) and (38h), and impose periodicity (being careful to include the jump in stress across $R = R_0 + \theta/2\pi$ given by (38j) and (38k)) to find

$$T^{(1)} = \int_0^{\theta/2\pi} F(r, R, \theta) dR + \int_{\theta/2\pi}^1 F(r, R, \theta) dR, \quad (45)$$

$$-\frac{\partial T^{(1)}}{\partial \theta} + \frac{1}{2\pi} \left[\sigma_{\theta\theta}^{(0)} \right]_{R_0+\theta/2\pi-}^{R_0+\theta/2\pi+} = \int_0^{\theta/2\pi} G(r, R, \theta) dR + \int_{\theta/2\pi}^1 G(r, R, \theta) dR. \quad (46)$$

Noting that $\sigma_{rr}^{(0)}$ and $\sigma_{r\theta}^{(0)}$ do not depend on R we can write (45) and (46) as

$$T^{(1)} = \frac{\partial(r\sigma_{rr}^{(0)})}{\partial r} + \frac{\partial\sigma_{r\theta}^{(0)}}{\partial \theta} - \int_0^{\theta/2\pi} \sigma_{\theta\theta}^{(0)} dR - \int_{\theta/2\pi}^1 \sigma_{\theta\theta}^{(0)} dR, \quad (47)$$

$$-\frac{\partial T^{(1)}}{\partial \theta} + \frac{1}{2\pi} \left[\sigma_{\theta\theta}^{(0)} \right]_{R_0+\theta/2\pi-}^{R_0+\theta/2\pi+} = \frac{\partial(r\sigma_{r\theta}^{(0)})}{\partial r} + \sigma_{r\theta}^{(0)} + \int_0^{\theta/2\pi} \frac{\partial\sigma_{\theta\theta}^{(0)}}{\partial \theta} dR + \int_{\theta/2\pi}^1 \frac{\partial\sigma_{\theta\theta}^{(0)}}{\partial \theta} dR. \quad (48)$$

Note that, by (40), the hoop stress, $\sigma_{\theta\theta}^{(0)}$, can be written in terms of the radial stress, $\sigma_{rr}^{(0)}$, which does not depend on R , and the material properties λ , μ , α and α_s .

Differentiating (47) with respect to θ and adding the result to (48) gives

$$\frac{\partial^2(r\sigma_{rr}^{(0)})}{\partial r\partial\theta} + \frac{\partial^2\sigma_{r\theta}^{(0)}}{\partial\theta^2} + \frac{\partial(r\sigma_{r\theta}^{(0)})}{\partial r} + \sigma_{r\theta}^{(0)} = 0. \quad (49)$$

We can then substitute (43) and (44) into (49) to obtain an equation in terms of $u^{(0)}$ and $v^{(0)}$. Finally we can use the inextensibility condition (37i) with (37b) to obtain a single equation for $v^{(0)}$. This equation is a fourth-order constant-coefficient PDE

$$\left(\int_0^1 \frac{1}{\mu} dR\right) \frac{\partial}{\partial r} \left(r \frac{\partial^3 v^{(0)}}{\partial r \partial \theta^2}\right) = \left(\int_0^1 \frac{1}{(\lambda + 2\mu)} dR\right) \left(-\frac{1}{r} \frac{\partial^4 v^{(0)}}{\partial \theta^4} - \frac{2}{r} \frac{\partial^2 v^{(0)}}{\partial \theta^2} + \frac{\partial}{\partial r} \left(r \frac{\partial v^{(0)}}{\partial r}\right) - \frac{v^{(0)}}{r}\right). \quad (50)$$

We need to solve (50) subject to matching conditions with the boundary layers near $r = 1$ and $r = r_0$. In these boundary layers, as discussed in the following sections, the displacements are small, of $\mathcal{O}(\delta)$, and remain bounded, the matching condition is $v^{(0)} \rightarrow 0$ as $r \rightarrow 1$ and $r \rightarrow r_0$. The solution of (50) with zero boundary data is just $v^{(0)} \equiv 0$, so that the complete leading-order outer solution is

$$u^{(0)} = \alpha_s r, \quad (51)$$

$$v^{(0)} = 0, \quad (52)$$

$$\sigma_{rr}^{(0)} = \int_0^1 \frac{(\alpha_s - \alpha)(3\lambda + 2\mu)}{(\lambda + 2\mu)} dy \left(\int_0^1 \frac{1}{(\lambda + 2\mu)} dy\right)^{-1}, \quad (53)$$

$$\sigma_{\theta\theta}^{(0)} = \frac{\lambda}{\lambda + 2\mu} \sigma_{rr}^{(0)} + \frac{2\mu(\alpha_s - \alpha)(3\lambda + 2\mu)}{\lambda + 2\mu}, \quad (54)$$

$$\sigma_{r\theta}^{(0)} = 0, \quad (55)$$

$$T^{(0)} = 0, \quad (56)$$

with the first-order tension given by

$$T^{(1)} = \sigma_{rr}^{(0)} - \int_0^1 \sigma_{\theta\theta}^{(0)} dy. \quad (57)$$

Note that in general the leading-order displacements and radial and shear stresses, and the first two orders of the tension, are slowly varying functions (they only depend on the macroscale). However, if the material properties are non-constant, the leading-order hoop stress may vary rapidly across the matrix layer as well as on the macroscale. Also note that if the material properties are uniform through the matrix, then the integrals in (53) and (54) are very simple to evaluate; in this case (57) gives $T^{(1)} \equiv 0$.

3.2. Analysis in the surface region near $r = r_0$

We now discuss the behaviour of the solution in the surface region, that is, in the first few windings near $r = r_0$. We write $r = r_0 + \delta\rho$ and exploit the fact that, in

order to get a sensible balance in the inextensibility condition, (35i), the azimuthal displacement must be small. We expand the variables in powers of δ , with the azimuthal displacement given by

$$v \sim \delta v^{(1)} + \dots, \quad (58)$$

and assume all other variables are $\mathcal{O}(1)$. Recall that the inner surface of the spiral is taken to be stress free. At leading order in δ we find

$$0 = \frac{\partial u^{(0)}}{\partial \rho}, \quad (59a)$$

$$\varepsilon_{\theta\theta}^{(0)} = \frac{u^{(0)}}{r_0}, \quad (59b)$$

$$0 = \varepsilon_{\theta\theta}^{(0)} - \alpha_s \text{ on } \rho = \theta/2\pi, \quad (59c)$$

with solution $u^{(0)} = \alpha_s r_0$, which is just the inner limit of the outer solution (51). At the next order we find

$$\varepsilon_{rr}^{(0)} = \frac{\partial u^{(1)}}{\partial \rho}, \quad (60a)$$

$$\varepsilon_{\theta\theta}^{(1)} = \frac{1}{r_0} \left(\frac{\partial v^{(1)}}{\partial \theta} + u^{(1)} \right) - \frac{\alpha_s \rho}{r_0}, \quad (60b)$$

$$\varepsilon_{r\theta}^{(0)} = \frac{1}{2} \frac{\partial v^{(1)}}{\partial \rho}, \quad (60c)$$

$$\sigma_{rr}^{(0)} = (\lambda + 2\mu) \frac{\partial u^{(1)}}{\partial \rho} + 2\lambda\alpha_s - \alpha(3\lambda + 2\mu), \quad (60d)$$

$$\sigma_{\theta\theta}^{(0)} = \lambda \frac{\partial u^{(1)}}{\partial \rho} + (\lambda + 2\mu)\alpha_s + \lambda\alpha_s - \alpha(3\lambda + 2\mu), \quad (60e)$$

$$\sigma_{r\theta}^{(0)} = \mu \frac{\partial v^{(1)}}{\partial \rho}, \quad (60f)$$

$$0 = \frac{\partial}{\partial \rho} \left((\lambda + 2\mu) \frac{\partial u^{(1)}}{\partial \rho} + 2\lambda\alpha_s - \alpha(3\lambda + 2\mu) \right), \quad (60g)$$

$$0 = \frac{\partial}{\partial \rho} \left(\mu \frac{\partial v^{(1)}}{\partial \rho} \right), \quad (60h)$$

$$0 = \frac{1}{2\pi} \frac{\partial v^{(1)}}{\partial \rho} + \left(\frac{\partial v^{(1)}}{\partial \theta} + u^{(1)} \right) - \alpha_s \rho \quad \text{on } \rho = \theta/2\pi, \quad (60i)$$

$$\frac{1}{r_0} \frac{\partial T^{(0)}}{\partial \theta} = -\sigma_{r\theta}^{(0)}(\theta/2\pi, \theta) \quad \text{for } \rho = \theta/2\pi, 0 \leq \theta < 2\pi, \quad (60j)$$

$$\frac{T^{(0)}}{r_0} = \sigma_{rr}^{(0)}(\theta/2\pi, \theta) \quad \text{for } \rho = \theta/2\pi, 0 \leq \theta < 2\pi, \quad (60k)$$

$$\frac{1}{r_0} \frac{\partial T^{(0)}}{\partial \theta} = -\sigma_{r\theta}^{(0)}(\theta/2\pi, \theta) + \sigma_{r\theta}^{(0)}(\theta/2\pi, \theta - 2\pi) \quad \text{for } \rho = \theta/2\pi, \theta \geq 2\pi, \quad (60l)$$

$$\frac{T^{(0)}}{r_0} = \sigma_{rr}^{(0)}(\theta/2\pi, \theta) - \sigma_{rr}^{(0)}(\theta/2\pi, \theta - 2\pi) \quad \text{for } \rho = \theta/2\pi, \theta \geq 2\pi, \quad (60m)$$

with boundary conditions on the outer surface of the matrix layer given by

$$\sigma_{\theta\theta}^{(0)} = 0 \quad \text{on } \theta = 0, 0 < \rho < 1, \quad (60n)$$

$$\sigma_{r\theta}^{(0)} = 0 \quad \text{on } \theta = 0, 0 < \rho < 1. \quad (60o)$$

Note that the jump conditions on the reinforcing sheet on the inner surface, (60j) and (60k) where $\rho = \theta/2\pi$, $0 < \theta < 2\pi$, must be treated differently from those in the interior, (60l) and (60m) where $\rho = \theta/2\pi$, $2\pi < \theta$. We separately write boundary conditions (60n) and (60o) on the surface of the matrix at the end of the spiral where $0 < \rho < 1$, $\theta = 0$.

Integrating (60g) and (60h) gives

$$u^{(1)} = \int_{\frac{\theta}{2\pi}}^{\rho} \frac{\alpha(3\lambda + 2\mu) - 2\lambda\alpha_s}{(\lambda + 2\mu)} d\rho + f_1(\theta) \int_{\frac{\theta}{2\pi}}^{\rho} \frac{d\rho}{\lambda + 2\mu} + f_2(\theta), \quad (61)$$

$$v^{(1)} = g_1(\theta) \int_{\frac{\theta}{2\pi}}^{\rho} \frac{d\rho}{\mu} + g_2(\theta), \quad (62)$$

with

$$\sigma_{rr}^{(0)} = f_1(\theta), \quad (63)$$

$$\sigma_{\theta\theta}^{(0)} = \frac{\lambda}{\lambda + 2\mu} f_1(\theta) + \frac{2\mu(\alpha_s - \alpha)(3\lambda + 2\mu)}{\lambda + 2\mu}, \quad (64)$$

$$\sigma_{r\theta}^{(0)} = g_1(\theta), \quad (65)$$

where we have introduced the arbitrary functions arising from the integration, $f_1(\theta)$, $f_2(\theta)$, $g_1(\theta)$, and $g_2(\theta)$, in order to simplify the subsequent analysis. Substituting $u^{(1)}$ and $v^{(1)}$ into the inextensibility condition (60i), we obtain

$$g_2'(\theta) + f_2(\theta) = \frac{\alpha_s \theta}{2\pi}. \quad (66)$$

The tension conditions (60j)–(60m) give

$$\frac{1}{r_0} \frac{\partial T^{(0)}}{\partial \theta} = -g_1(\theta) \quad \text{for } 0 \leq \theta < 2\pi, \quad (67)$$

$$\frac{T^{(0)}}{r_0} = f_1(\theta) \quad \text{for } 0 \leq \theta < 2\pi, \quad (68)$$

$$\frac{1}{r_0} \frac{\partial T^{(0)}}{\partial \theta} = -g_1(\theta) + g_1(\theta - 2\pi) \quad \text{for } \theta \geq 2\pi, \quad (69)$$

$$\frac{T^{(0)}}{r_0} = f_1(\theta) - f_1(\theta - 2\pi) \quad \text{for } \theta \geq 2\pi. \quad (70)$$

Eliminating $T^{(0)}$ gives

$$f_1'(\theta) + g_1(\theta) = 0 \quad 0 \leq \theta < 2\pi, \quad (71)$$

$$f_1'(\theta) + g_1(\theta) = f_1'(\theta - 2\pi) + g_1(\theta - 2\pi) \quad \theta \geq 2\pi, \quad (72)$$

which implies that

$$f_1' + g_1 = 0 \quad \text{for all } \theta \geq 0. \quad (73)$$

Continuity of displacement at the reinforcing sheet gives

$$f_2(\theta) = \hat{\Sigma} - 2\alpha_s \hat{L} + \hat{M}^{-1} f_1(\theta - 2\pi) + f_2(\theta - 2\pi) \quad \theta \geq 2\pi, \quad (74)$$

$$g_2(\theta) = \hat{\mu}^{-1} g_1(\theta - 2\pi) + g_2(\theta - 2\pi) \quad \theta \geq 2\pi, \quad (75)$$

where we have introduced the following notation to represent the average material properties

$$\hat{\Sigma} = \int_0^1 \frac{\alpha(y)(3\lambda(y) + 2\mu(y))}{\lambda(y) + 2\mu(y)} dy, \quad (76)$$

$$\hat{\mu} = \left(\int_0^1 \frac{1}{\mu(y)} dy \right)^{-1}, \quad (77)$$

$$\hat{L} = \int_0^1 \frac{\lambda(y)}{\lambda(y) + 2\mu(y)} dy, \quad (78)$$

$$\hat{M} = \left(\int_0^1 \frac{1}{\lambda(y) + 2\mu(y)} dy \right)^{-1}, \quad (79)$$

and we have used the fact that the material properties are periodic in $\rho - \theta/2\pi$ with unit period. Here \hat{M} represents an effective constrained (or P-wave) modulus, \hat{L} an effective ratio of the first Lamé parameter to the constrained modulus, $\hat{\mu}$ an effective shear modulus, and $\hat{\Sigma}$ an effective product of the expansion coefficient, shear modulus and reciprocal of the constrained modulus. The parameter $\hat{\Sigma}$ can be interpreted as an effective strain due to the prescribed expansion. For constant material properties we have $\hat{M} = M = \lambda + 2\mu$, $\hat{L} = \lambda/M$, $\hat{\mu} = \mu$, and $\hat{\Sigma} = 3\alpha K/M$, where $K = \lambda + 2\mu/3$ is the bulk modulus.

The conditions at the matrix outer surface (60n) and (60o) give

$$\frac{\lambda}{\lambda + 2\mu} f_1(0) + \frac{2\mu(\alpha_s - \alpha)(3\lambda + 2\mu)}{\lambda + 2\mu} = 0, \quad (80)$$

$$g_1(0) = 0, \quad (81)$$

$$T^{(0)}(0) = 0. \quad (82)$$

We will find later that these three conditions cannot simultaneously be imposed on the problem, and this indicates we must consider the end-of-winding region, near $(r, \theta) = (r_0, 0)$, which we look at later in Section 3.3. However, behaviour in the end-of-winding region indicates that for the problem here we should only impose (82), that the tension is zero.

In summary, the governing equations for $g_1(\theta)$, $g_2(\theta)$, $f_1(\theta)$, and $f_2(\theta)$ are

$$g_2' + f_2 = \frac{\alpha_s \theta}{2\pi} \quad \theta \geq 0, \quad (83)$$

$$f_1' + g_1 = 0 \quad \theta \geq 0, \quad (84)$$

$$f_2(\theta) = \hat{\Sigma} - 2\alpha_s \hat{L} + \hat{M}^{-1} f_1(\theta - 2\pi) + f_2(\theta - 2\pi) \quad \theta \geq 2\pi, \quad (85)$$

$$g_2(\theta) = \hat{\mu}^{-1} g_1(\theta - 2\pi) + g_2(\theta - 2\pi) \quad \theta \geq 2\pi, \quad (86)$$

and we now seek to find analytic expressions for the solutions, taking great care to account for which region of θ is being considered in each equation. We shall ensure that the solution is continuous in θ and periodic as $\theta \rightarrow \infty$, and will find this requires that the solution decays to a constant in order to match with the outer solution.

We start by considering the region $\theta \geq 2\pi$ and use (83) in (85) to get

$$\hat{\Sigma} - 2\alpha_s \hat{L} + \hat{M}^{-1} f_1(\theta - 2\pi) = g_2'(\theta - 2\pi) - g_2'(\theta) + \alpha_s, \quad (87)$$

then differentiate (86) and use (84) to get

$$-\hat{\mu}^{-1} f_1''(\theta - 2\pi) = g_2'(\theta) - g_2'(\theta - 2\pi). \quad (88)$$

We can now add (87) to (88) to get

$$\hat{\Sigma} - 2\alpha_s \hat{L} - \alpha_s + \hat{M}^{-1} f_1(\theta - 2\pi) = \hat{\mu}^{-1} f_1''(\theta - 2\pi). \quad (89)$$

Note that we can define a new effective material property which depends on the difference between the expansion coefficient in the matrix and the reinforcing sheet as

$$\hat{\Sigma}_{\text{diff}} = \hat{\Sigma} - 2\alpha_s \hat{L} - \alpha_s = \int_0^1 \frac{(\alpha(y) - \alpha_s)(3\lambda(y) + 2\mu(y))}{\lambda(y) + 2\mu(y)} dy. \quad (90)$$

As the effective material parameters are constants, the solution which is bounded at infinity is

$$f_1(\theta) = -\hat{M} \hat{\Sigma}_{\text{diff}} + A \hat{M} e^{-\omega(\theta+2\pi)}, \quad \text{where} \quad \omega^2 = \frac{\hat{\mu}}{\hat{M}}, \quad (91)$$

where A is an arbitrary constant. Note that the decay length, ω , depends only on the material properties λ and μ , and not on the prescribed expansion α . Now, (84) gives

$$g_1 = \omega A \hat{M} e^{-\omega(\theta+2\pi)}. \quad (92)$$

Substituting (91) into (85) we find for $\theta \geq 2\pi$ that

$$f_2(\theta) - f_2(\theta - 2\pi) = A e^{-\omega\theta} + \alpha_s \quad (93)$$

with solution

$$f_2(\theta) = F_2(\theta) + \frac{\alpha_s \theta}{2\pi} + C e^{-\omega\theta}, \quad (94)$$

where $A = C(1 - e^{2\pi\omega})$ and F_2 is an arbitrary 2π -periodic function of θ . Now (83) gives

$$g_2 = \int_0^\theta F_2(\bar{\theta}) d\bar{\theta} + D + \frac{C}{\omega} e^{-\omega\theta}. \quad (95)$$

Matching requires g_2 to be periodic for large θ , so that F_2 must have zero mean:

$$\int_0^{2\pi} F_2(\bar{\theta}) d\bar{\theta} = 0. \quad (96)$$

Finally, from (68) and (70) we determine the tension

$$T^{(0)} = r_0 \hat{M} \left(-\hat{\Sigma}_{\text{diff}} + A e^{-\omega(\theta+2\pi)} \right) \quad 0 \leq \theta < 2\pi, \quad (97)$$

$$T^{(0)} = r_0 \hat{M} A \left(e^{-\omega(\theta+2\pi)} - e^{-\omega\theta} \right) \quad \theta \geq 2\pi. \quad (98)$$

We now impose the condition $T^{(0)}(0) = 0$ (the boundary condition (82)) to give

$$A e^{-2\pi\omega} = \hat{\Sigma}_{\text{diff}}, \quad (99)$$

so that the tension is given by

$$T^{(0)} = -r_0 \hat{\Sigma}_{\text{diff}} \hat{M} (1 - e^{-\omega\theta}) \quad 0 \leq \theta < 2\pi, \quad (100)$$

$$T^{(0)} = -r_0 \hat{\Sigma}_{\text{diff}} \hat{M} e^{-\omega\theta} (e^{2\pi\omega} - 1) \quad \theta \geq 2\pi. \quad (101)$$

To determine f_2 and g_2 , and therefore $u^{(1)}$ and $v^{(1)}$, we need to find F_2 . After some algebra, we find a solvability condition on the next-order equations that requires $D = 0$.

To summarise, in the surface region, the displacements are $u = \alpha_s r_0 + \delta u^{(1)}$ and $v = \delta v^{(1)}$, where the $\mathcal{O}(\delta)$ terms are given by (61) and (62), and the leading order stresses are given by (63) – (65). All of these are expressed in terms of the functions $f_{1,2}(\theta)$ and $g_{1,2}(\theta)$, which are given by equations (91), (92), (94), and (95).

3.3. Analysis in the end-of-winding region, near $r = r_0, \theta = 0$

Since we are unable to impose all three boundary conditions (80)–(82) on the solution in the surface region we now consider a small end-of-winding region near the end of the reinforcing sheet, as shown in Figure 3. In this region we have significant stresses due to the jump along the inextensible reinforcing sheet from a section with matrix on either side to a section which is stress free on one side. The finite thickness of the matrix layer is also important as it sets the radial length scale as well as the azimuthal lengthscale. In this region we take $r = r_0 + \delta\rho$, $\theta = \delta\Theta/r_0$, and take $u = \alpha_s r_0 + \delta U$, $v = \delta V$.

To simplify the analysis, we introduce new variables \tilde{U} and \tilde{V} in each layer $n <$

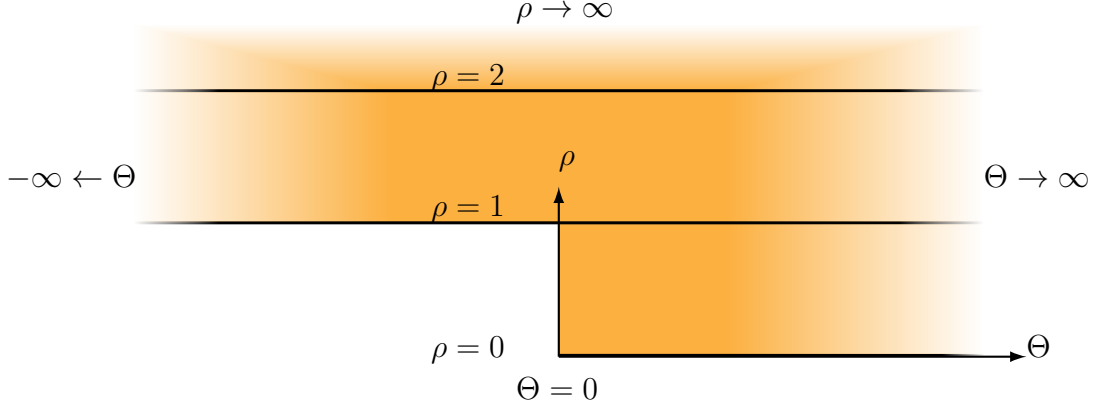


Figure 3: Representation of boundary layer near $r = r_0$, $\theta = 0$.

$\rho < n + 1$, for $n = 0, 1, 2, \dots$, such that

$$U = (\omega \hat{M}(\hat{\Sigma}_{\text{diff}} + \alpha_s))\tilde{U} + \int_n^\rho \frac{\alpha(3\lambda + 2\mu) - 2\lambda\alpha_s}{\lambda + 2\mu} d\rho + f_1(2n\pi) \int_n^\rho \frac{d\rho}{\lambda + 2\mu} + f_2(2n\pi), \quad (102)$$

$$V = (\omega \hat{M}(\hat{\Sigma}_{\text{diff}} + \alpha_s))\tilde{V} + g_1(2n\pi) \int_n^\rho \frac{d\rho}{\mu} + g_2(2n\pi), \quad (103)$$

where we note that, to leading order, the material properties are functions of the radial coordinate ρ only. Here we have written the displacements U and V as a combination of the surface region solution near r_0 (these are only functions of ρ in this small region) and new unknown displacements \tilde{U} and \tilde{V} . The scaling coefficient $\omega \hat{M}(\hat{\Sigma}_{\text{diff}} + \alpha_s)$ has been introduced so that the forcing term in the shear stress boundary condition at $\Theta = 0$ for \tilde{U} and \tilde{V} , (104h), is equal to one. In order to match on to the outer solution we must have that $\tilde{U}, \tilde{V} \rightarrow 0$ as $\Theta \rightarrow \pm\infty$.

Expanding \tilde{U} and \tilde{V} in δ in the usual way, at leading order we get

$$\frac{\partial}{\partial \Theta} \left((\lambda + 2\mu) \frac{\partial \tilde{V}}{\partial \Theta} + \lambda \frac{\partial \tilde{U}}{\partial \rho} \right) + \frac{\partial}{\partial \rho} \left(\mu \left(\frac{\partial \tilde{V}}{\partial \rho} + \frac{\partial \tilde{U}}{\partial \Theta} \right) \right) = 0, \quad (104a)$$

$$\frac{\partial}{\partial \Theta} \left(\mu \left(\frac{\partial \tilde{V}}{\partial \rho} + \frac{\partial \tilde{U}}{\partial \Theta} \right) \right) + \frac{\partial}{\partial \rho} \left(\lambda \frac{\partial \tilde{V}}{\partial \Theta} + (\lambda + 2\mu) \frac{\partial \tilde{U}}{\partial \rho} \right) = 0, \quad (104b)$$

$$\frac{\partial T}{\partial \Theta} = 0, \quad (104c)$$

$$\frac{\partial \tilde{V}}{\partial \Theta} = 0, \quad \text{on } \rho = n \geq 0, \quad (104d)$$

$$\tilde{V} = 0, \quad \text{on } \rho = n \geq 0, \quad (104e)$$

$$\frac{\partial \tilde{U}}{\partial \rho} = 0, \quad \text{on } \rho = 0, 0 < \Theta < \infty, \quad (104f)$$

$$(\lambda + 2\mu) \frac{\partial \tilde{V}}{\partial \Theta} + \lambda \frac{\partial \tilde{U}}{\partial \rho} = F_{\theta\theta}, \quad \text{on } \Theta = 0, 0 < \rho < 1, \quad (104g)$$

$$\mu \left(\frac{\partial \tilde{V}}{\partial \rho} + \frac{\partial \tilde{U}}{\partial \Theta} \right) = -1, \quad \text{on } \Theta = 0, \ 0 < \rho < 1, \quad (104h)$$

$$\frac{\partial \tilde{U}}{\partial \rho} = 0, \quad \text{on } \rho = 1, \ -\infty < \Theta < 0, \quad (104i)$$

$$\left[\frac{\partial \tilde{U}}{\partial \rho} \right]_{-}^{+} = 0, \quad \text{on } \rho = 1, \ 0 < \Theta < \infty, \quad (104j)$$

$$\left[\frac{\partial \tilde{U}}{\partial \rho} \right]_{-}^{+} = 0, \quad \text{on } \rho = n \geq 2, \ -\infty < \Theta < \infty, \quad (104k)$$

$$\left[\tilde{U} \right]_{-}^{+} = \left[\tilde{V} \right]_{-}^{+} = 0, \quad \text{on } \rho = n \geq 1, \quad (104l)$$

with

$$F_{\theta\theta} = \frac{\hat{\mu}^{1/2}}{\hat{M}^{1/2}(\hat{\Sigma}_{\text{diff}} + \alpha_s)} \frac{1}{\lambda + 2\mu} (2\mu\alpha(3\lambda + 2\mu) + \lambda\alpha_s(\lambda - 2\mu)). \quad (104m)$$

Note, that this problem is readily identified as the equations resulting from considering a linear elastic material in a Cartesian system (Θ, ρ) . Because of the layered strip geometry in the end-of-winding boundary layer and the step in the outer surface, as shown in Figure 3, this problem needs to be solved numerically, but this is straightforward using standard finite element software. Crucially, the results show that, of the three possible boundary conditions, the appropriate matching condition to impose on the bulk solution is that the tension goes to zero, as used earlier.

4. Results

In the preceding analysis we treated the general case in which the parameters may vary rapidly through the layers and macroscopically, with radius. We will now present results in the simplest case in which the parameters α , λ , and μ are all constant, using the dimensionless parameter values provided in Table 1. In order to demonstrate the effect of allowing the reinforcing sheet to expand we consider two cases: $\alpha_s = 0$, where the sheet does not expand at all, and $\alpha_s = 0.5$, where the reinforcing sheet expands half as much as the matrix. If all parts of the spiral expand identically ($\alpha = \alpha_s$) then the entire structure is stress-free.

In order to assess the efficacy of the simplified model developed in the previous sections we will show a comparison with numerical solutions of the “full” problem found using COMSOL. The COMSOL model solves the linear elasticity problem with a prescribed expansion, i.e. (21), (22) and (34), but includes a reinforcing sheet of a small but finite thickness $h_s \ll \delta$. The dimensionless Young’s modulus, E_s , and thickness of the reinforcing sheet was selected so that the bending stiffness was small compared to the tension, which was in turn small compared to the stiffness, i.e.

$$\frac{E_s h_s^3}{r_0^2} \ll E(\alpha - \alpha_s) r_0 \ll E_s h_s, \quad (105)$$

Parameter	Description	Value
r_0	Inner radius	0.25
N	Number of winds	10
δ	Layer thickness	0.075
λ	First Lamé parameter	2
μ	Shear modulus	1
α	Matrix expansion coefficient	1
α_s	Reinforcing sheet expansion coefficient	0.0 or 0.5
$\hat{\Sigma}$	Effective matrix expansion strain measure	2
$\hat{\Sigma}_{\text{diff}}$	Effective differential expansion strain measure	2 or 1
$\hat{\mu}$	Effective shear modulus	1
\hat{M}	Effective constrained modulus	4

Table 1: Dimensionless parameters used in comparison between COMSOL solutions and asymptotic solutions. The layer thickness was computed as $\delta = (1 - r_0)/N$.

where E is the dimensionless Young’s modulus of the matrix. Satisfying this inequality ensures the finite thickness reinforcing sheet behaves as though it is inextensible. Simulations were performed for varying values of E_s and h_s to ensure the solution was independent of the choice of values, provided (105) is satisfied. For the results presented here we used $E_s/E = 10^4$ and $h_s = 0.01\delta$. The spiral domain was discretised using the Finite Element Method with quadratic basis elements. A total of 49692 mesh elements were included, leading to around 8 elements across the thickness of each winding, and the solver used a relative tolerance of 10^{-3} . The mesh and solver tolerances were refined until no graphical changes in the solution were observed.

In our comparisons we will show the “surface solution” which is valid in the surface layer near $r = r_0$ and in the bulk, and a “surface-end composite” solution valid in the bulk, the surface and the end-of-winding regions. The composite solution is found in the usual way for asymptotic expansions by adding the solutions across the different regions, and subtracting off their common part (see, e.g. [11]). Note that the surface solution is uniformly valid in the surface region and the bulk region. However, one must take care to note that terms that are linear in θ in the surface region, as in (94), match onto terms that are linear in r in the bulk.

Figure 4 gives a comparison of the asymptotic and numerical solutions for the radial displacements for $\alpha_s = 0$ and $\alpha_s = 0.5$. In both cases we see that the surface solution accurately captures the exponential decay in these functions, but there are additional “spikes” in the numerical solution as we pass through $\theta = 2n\pi$, $n = 1, 2, \dots$. The surface-end solution gives the correct exponential decay and predicts both the position and the amplitude of the spikes in the solution as we pass through $\theta = 2n\pi$. However, there are additional oscillations in the solution that are not captured by this surface-end solution. In particular, the surface-end solution near $\theta = 2\pi$ decays monotonically from the spike to the exponential behaviour, unlike the

COMSOL solution which decays then grows. The most obvious difference between the two cases is that when $\alpha_s = 0$ the displacement decays to zero as θ increases, whereas when $\alpha_s = 0.5$ the displacement increases linearly with θ . The expansion of the reinforcing sheet admits a linear radial expansion in the bulk, see (51). In this case we see that the entire spiral moves radially outwards as it expands, whereas in the case $\alpha_s = 0$ we find that the reinforcing sheet confines the matrix material in the bulk and all of the displacement occurs within the first wind.

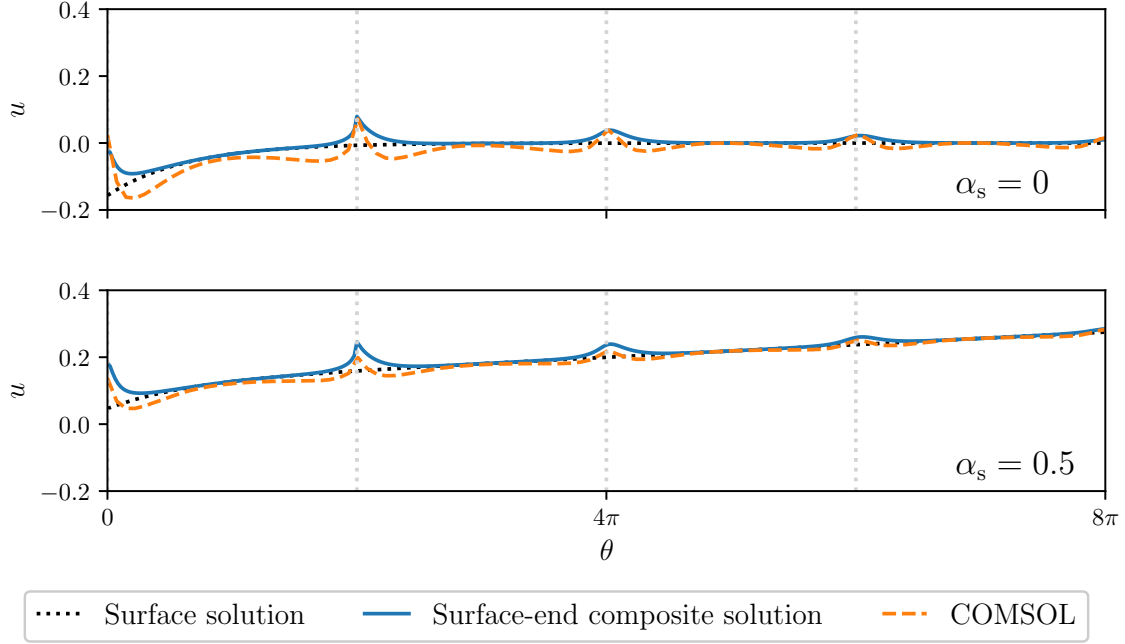


Figure 4: A comparison of the calculated (COMSOL) and predicted (asymptotic analysis) radial displacement u for the cases $\alpha_s = 0$ (upper panel) and $\alpha_s = 0.5$ (lower panel). The displacements are evaluated at $r = r_0 + \delta\theta/2\pi$ for $0 \leq \theta \leq 8\pi$.

Figure 5 shows a similar comparison for the azimuthal displacement. Here we observe that in both cases the displacement goes to zero as θ increases. Changing the prescribed expansion controls the maximum displacement at the end of the wind. In this we do not see the spikes as we pass through $\theta = 2n\pi$, but there are “ramps” around these points. Neither the surface nor composite solution predict these ramps. In the end-of-winding region, (104e) gives $\tilde{V} = 0$ on $\rho = n$, so we do not expect the composite solution to show the ramps, and suspect these appear in higher-order terms.

Figure 6 gives a comparison of the asymptotic and numerical solutions for the stresses and strains in the matrix layer when $\alpha_s = 0.5$. We observe that the stresses and strains may be large in the first wind, with an exponential decay as θ increases. Again there are spikes at $\theta = 2n\pi$ and the surface-end predicts these well, but does not show the slightly oscillatory behaviour between spikes. As θ increases, the normal strains decay to the prescribed expansion of the reinforcing sheet, α_s , and the shear strain decays to zero. Figure 7 shows the same comparison for $\alpha_s = 0$. We

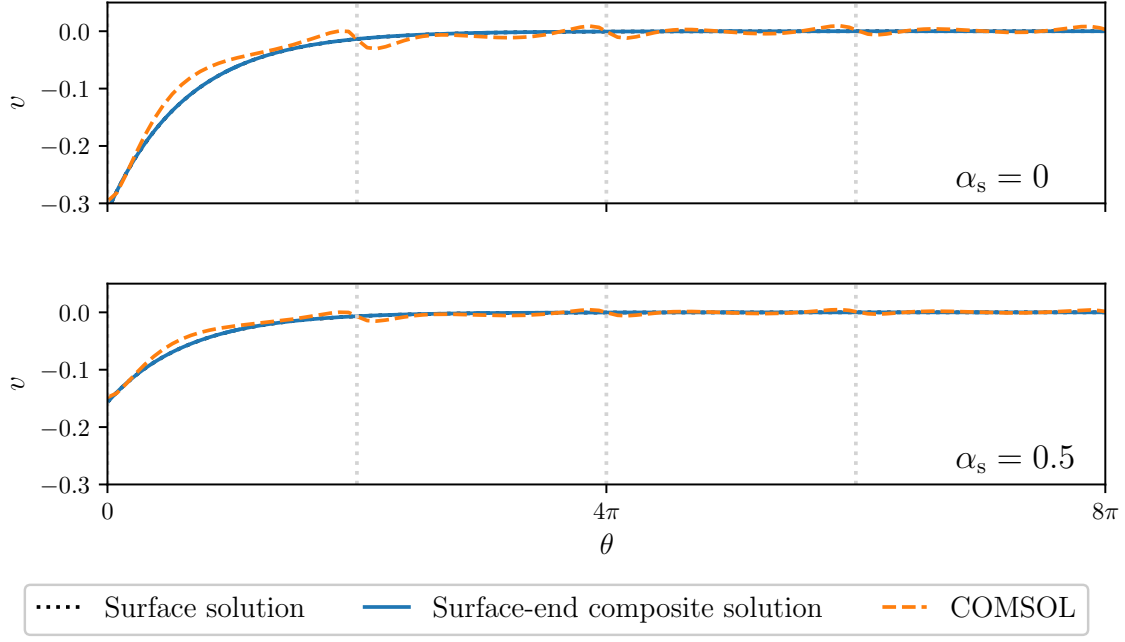


Figure 5: A comparison of the calculated (COMSOL) and predicted (asymptotic analysis) azimuthal displacement v for the cases $\alpha_s = 0$ (upper panel) and $\alpha_s = 0.5$ (lower panel). The displacements are evaluated at $r = r_0 + \delta\theta/2\pi$ for $0 \leq \theta \leq 8\pi$.

see the solution has all the same qualitative features but, since $\alpha_s = 0$, the strains must all go to zero in the bulk. We also observe that the magnitudes of the stresses and strains are altered. When the reinforcing sheet does not expand the material in the bulk is confined, so the matrix is under more compression. In both cases the shear stress goes to zero in the bulk.

Figure 8 gives a comparison of the tension in the reinforcing sheet as given by the surface solution (100)–(101) and as computed in COMSOL for the cases $\alpha_s = 0$ and $\alpha_s = 0.5$. We find that the surface layer solution predicts the initial exponential growth in tension in the first wind and that the maximum tension (compression) agrees with the COMSOL result. After the first wind the tension decays exponentially, with the COMSOL solution displaying a shoulder and small spikes in the tension that are not present in the surface layer solution. Here we see that, since the tension depends on the difference between the expansion coefficient in matrix and the reinforcing sheet, allowing the reinforcing sheet to expand reduces the peak tension.

It is important to note that the tension (100) – (101) is controlled by two products of dimensionless effective material properties, namely $\hat{\Sigma}_{\text{diff}}\hat{M}$ and $\hat{\mu}/\hat{M}$. Changes to the expansion coefficient in the matrix and/or the reinforcing sheet lead to changes in $\hat{\Sigma}_{\text{diff}}$, and changes in the elastic properties of the matrix lead to changes in all of the effective properties. Figure 9 shows the tension for various different values of $\hat{\Sigma}_{\text{diff}}\hat{M}$ and $\hat{\mu}/\hat{M}$. The top panel was generated by holding $\hat{\mu}/\hat{M}$ fixed and varying $\hat{\Sigma}_{\text{diff}}\hat{M}$. This was achieved by fixing the elastic properties μ and λ , so that $\hat{\mu}$ and \hat{M} were

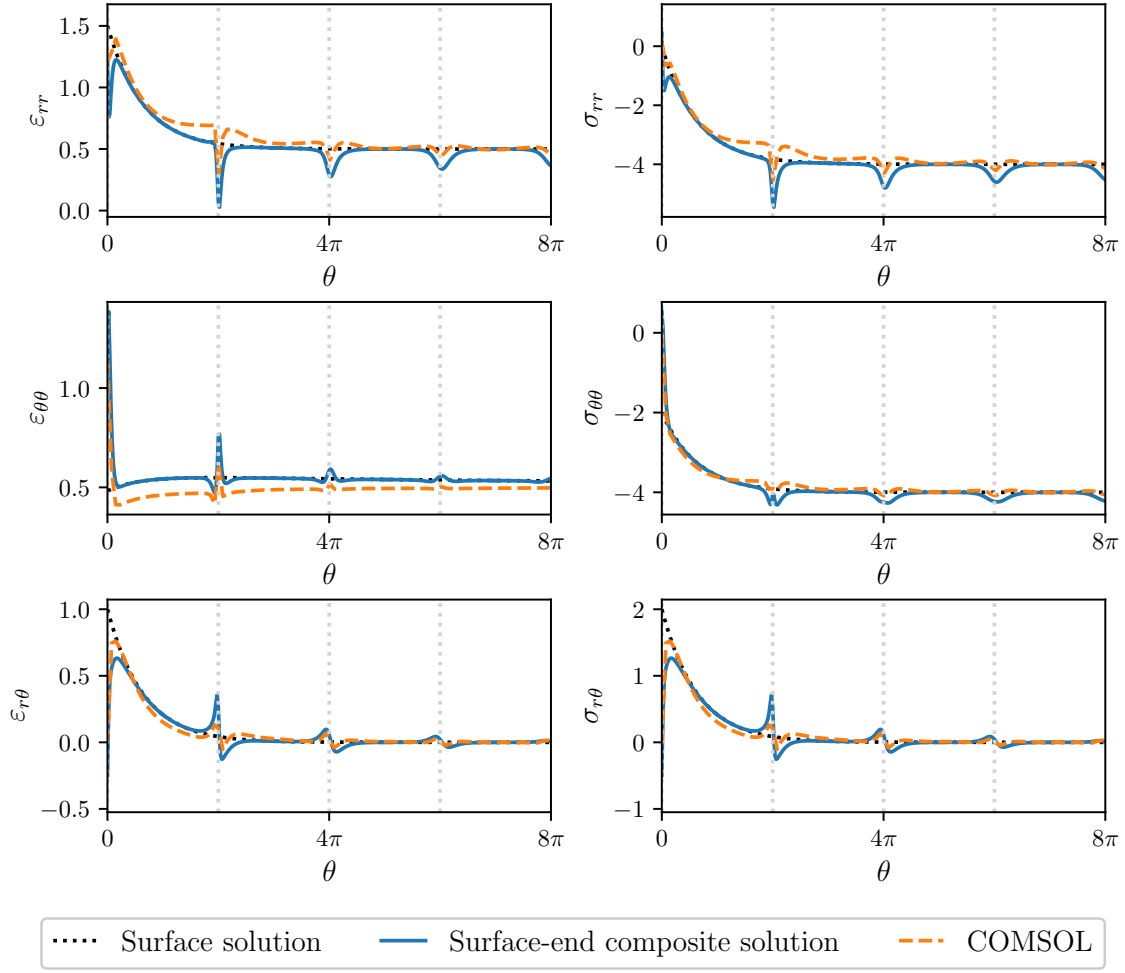


Figure 6: A comparison of the calculated (COMSOL) and predicted (asymptotic analysis) radial u and azimuthal v displacements, evaluated at $r = r_0 + \delta\theta/2\pi$ for $0 \leq \theta \leq 8\pi$. Here the reinforcing sheet expands with $\alpha_s = 0.5$.

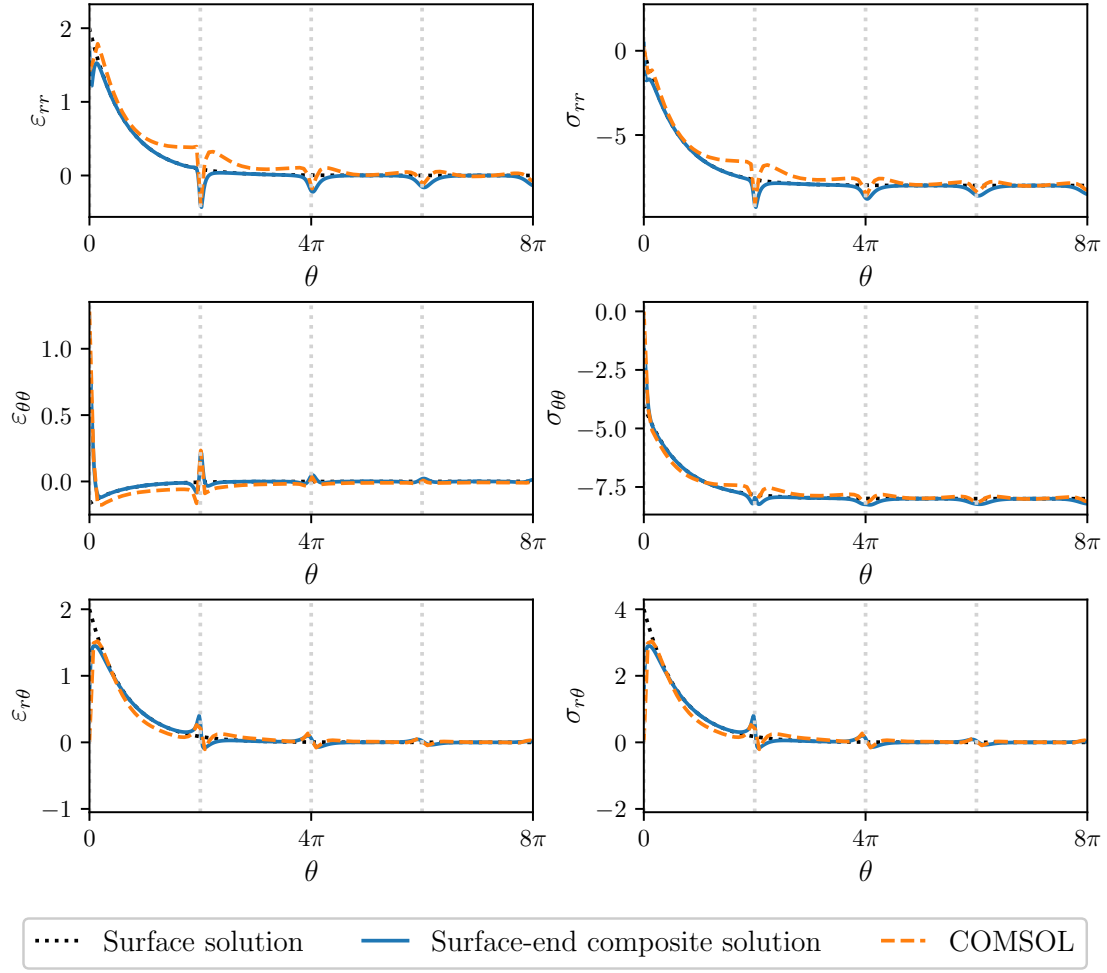


Figure 7: A comparison of the calculated (COMSOL) and predicted (asymptotic analysis) radial u and azimuthal v displacements, evaluated at $r = r_0 + \delta\theta/2\pi$ for $0 \leq \theta \leq 8\pi$. Here the reinforcing sheet does not expand ($\alpha_s = 0$).

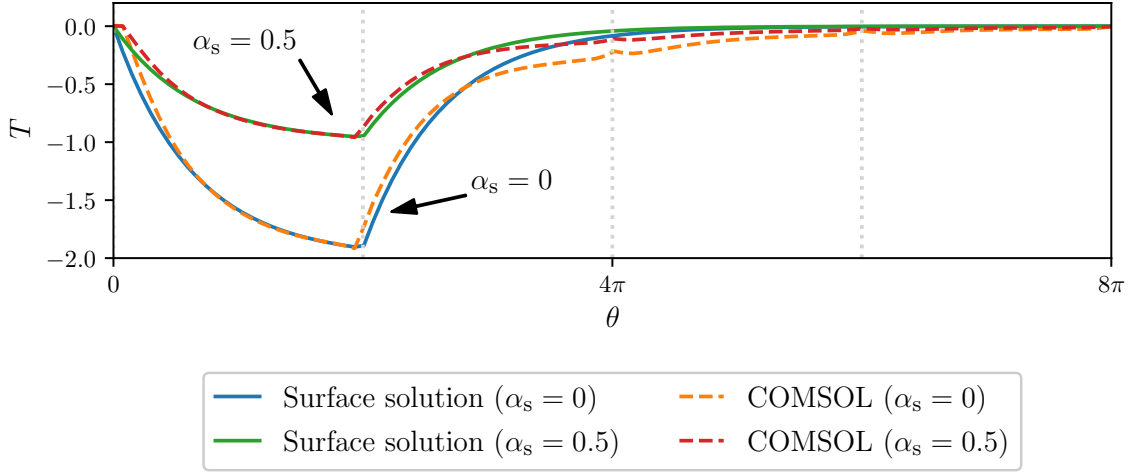


Figure 8: A comparison of the calculated (COMSOL) and predicted (asymptotic analysis) tension for the cases $\alpha_s = 0$ and $\alpha_s = 0.5$.

constant, and then varying $\hat{\Sigma}_{\text{diff}}$ which could represent a change in the expansion coefficient of the matrix, the reinforcing sheet, or both. The bottom panel was generated by holding μ and α_s fixed and then varying α and λ in such a way that $\hat{\Sigma}_{\text{diff}}\hat{M}$ remained constant. We observe that the maximum tension is controlled by the product $\hat{\Sigma}_{\text{diff}}\hat{M}$, whereas the decay length is controlled by the ratio $\hat{\mu}/\hat{M}$.

One useful practical result from the asymptotic solutions is that, given we have found an explicit expression for the tension, we can *a posteriori* compute an estimate for the strain in the reinforcing sheet (see [12]) as

$$\varepsilon_s = \frac{T^*}{E_s^* t_s^*}, \quad (106)$$

where E_s^* and t_s^* are the Young's modulus and thickness of the reinforcing sheet, respectively. Recall that the tension is per unit height, hence the reinforcing sheet thickness appears in (106) instead of the cross-sectional area.

5. Conclusion

In this work we have used multiple-scales homogenisation and boundary layer analysis to develop reduced order models describing the mechanics of spirally-wound layered materials containing a layered matrix and an inextensible reinforcing sheet, where both can expand isotropically. Our analysis exploited the thinness of each individual layer of the matrix material compared with the overall dimensions of the spiral structure. We demonstrated that the solution is made up of three regions: i) an outer region that makes up the bulk of the domain, ii) an inner region near the surface of the spiral which extends a couple of windings into the structure, and iii) a further boundary layer region which extends only a small radial distance and small angle from the end of the winding. A similar boundary layer structure exists

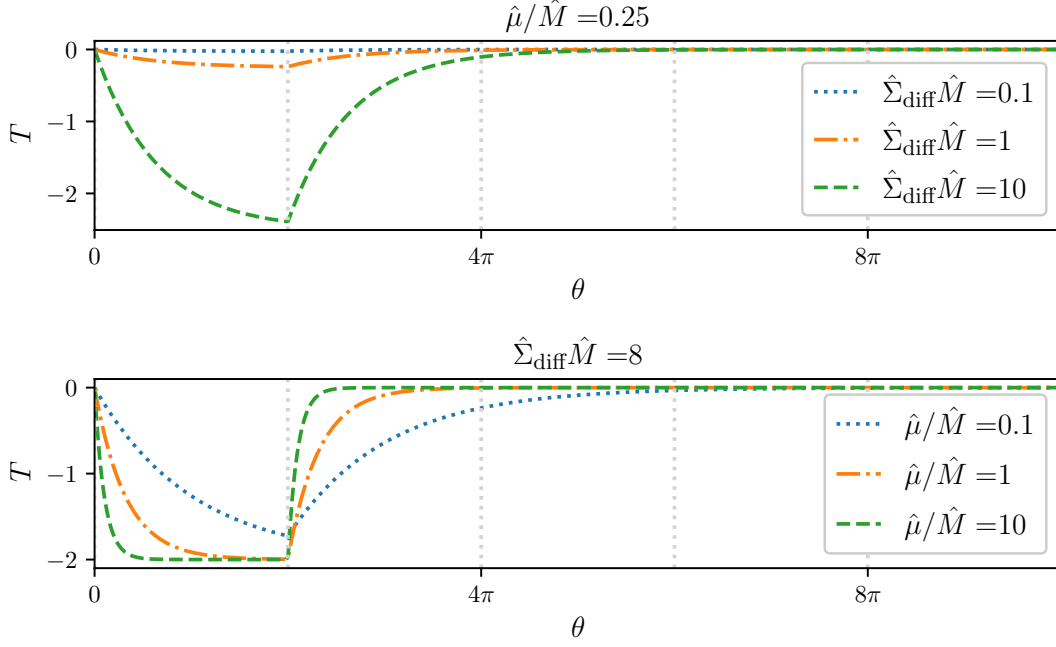


Figure 9: The surface solution for the tension in the reinforcing sheet with different values of the dimensionless groupings $\hat{\Sigma}_{\text{diff}}\hat{M}$ and $\hat{\mu}/\hat{M}$.

near the outer surface of the spiral in which the same analysis holds, however we did not give the details here. We constructed composite solutions valid across each of the three regions and presented comparisons of these composite solutions with numerical solutions of the original problem found using COMSOL. The comparisons demonstrated that our simple, closed-form expressions for the displacement, strains, stresses and tension agreed favourably with the numerical solution while avoiding computational issues such as those related to meshing the complicated spiral structure, as in the Finite Element Method. Evaluating the expressions for the surface solution comes with almost zero computational cost, and the numerical solution of the end-of-winding problem took on the order of seconds, so even the composite solution offers a significant speed-up compared with the full Finite Element simulation which took on the order of minutes. For a more realistic battery geometry, in which the material properties vary with distance through the layer, the speed-up would be even greater. Further, the surface solution is sufficient to predict the tension and general form of the stresses and strains – we only need the composite solution to predict the “spikes” – so we can therefore predict the key outputs by simply evaluating closed-form expressions.

The analysis in the outer region gave the surprisingly simple result that, to leading order, there is no tension in the reinforcing sheet and that the shear stress in the matrix material is also zero. The reinforcing sheet acts to confine the movement of the matrix material so that when the reinforcing sheet does not expand ($\alpha_s = 0$) the entire structure does not move. If the reinforcing sheet does expand then a simple radial displacement of the matrix material is admitted.

At first sight it seems surprising that the tension in the reinforcing sheet is zero in the bulk, even as it acts to confine the expanding matrix material. However, this can be understood by realising that, in the bulk, the structure behaves as though the reinforcing sheet forms concentric circles within the matrix material. In that case all the stress of resisting the expansion would be taken up by a constant nonzero tension in the outermost and innermost circles, with zero tension in all interior circles.

Our analysis of the boundary layer comprising the first few winds highlights the difference between concentric circles and a spiral. We showed that the tension builds up during the first wind and then decays exponentially, with a maximum at the end of the first wind. The location of the maximum tension qualitatively agrees with the location of buckling behaviour observed in spirally-wound lithium-ion batteries [8, 4, 5, 6]. A further boundary layer near the end of the windings allowed the asymptotic solution to capture additional features seen in the numerical solution, and interestingly the effect of this small boundary layer propagates to subsequent winds, giving interesting modulations to the solution on every loop of the spiral.

The work presented in this paper not only treats a novel mathematical problem, but also lays the foundations for future work related to the mechanical modelling of real-life products such as spirally-wound lithium-ion cells. Here we assumed that the expansion of all the materials was known, but in practice a model of this kind may be coupled to an additional problem to determine the local expansion. For instance, the expansion may be due to thermal effects and the problem presented here would need to be coupled to the heat equation. The simple expressions for the displacements and stresses found in this work readily enable such a coupling, and allow mechanical effects to be included in multiphysics models without any significant computational overhead.

6. Acknowledgements

This publication is based on work supported with funding provided by the EPSRC Faraday Institution Multiscale Modelling project (EP/S003053/1, grant number FIRG025). The authors appreciate useful discussions with Dr Toby Kirk.

7. Competing Interests

The authors have no competing interests to declare.

References

- [1] S. Psaltis, R. Timms, C. Please, S. J. Chapman, Homogenization of spirally wound high-contrast layered materials, *SIAM Journal on Applied Mathematics* 82 (1) (2022) 168–193. doi:10.1137/20M1377904.
- [2] J. Cannarella, C. B. Arnold, Stress evolution and capacity fade in constrained lithium-ion pouch cells, *Journal of Power Sources* 245 (2014) 745–751. doi:10.1016/j.jpowsour.2013.06.165.

- [3] L. K. Willenberg, P. Dechent, G. Fuchs, D. U. Sauer, E. Figgemeier, High-precision monitoring of volume change of commercial lithium-ion batteries by using strain gauges, *Sustainability* 12 (2) (2020) 557. doi:10.3390/SU12020557.
- [4] T. Waldmann, S. Gorse, T. Samtleben, G. Schneider, V. Knoblauch, M. Wohlfahrt-Mehrens, A mechanical aging mechanism in lithium-ion batteries, *Journal of The Electrochemical Society* 161 (10) (2014) A1742. doi:10.1149/2.1001410jes.
- [5] M. D. R. Kok, J. B. Robinson, J. S. Weaving, Anmol Jnawali, Martin Pham, Francesco Iacoviello, D. J. L. Brett, P. R. Shearing, Virtual unrolling of spirally-wound lithium-ion cells for correlative degradation studies and predictive fault detection, *Sustainable Energy & Fuels* 3 (11) (2019) 2972–2976. doi:10.1039/C9SE00500E.
- [6] A. Pfrang, A. Kersys, A. Kriston, D. U. Sauer, C. Rahe, S. Käbitz, E. Figgemeier, Geometrical inhomogeneities as cause of mechanical failure in commercial 18650 lithium ion cells, *Journal of The Electrochemical Society* 166 (15) (2019) A3745. doi:10.1149/2.0551914jes.
- [7] J. Luo, C. Y. Dai, Z. Wang, K. Liu, W. G. Mao, D. N. Fang, X. Chen, In-situ measurements of mechanical and volume change of LiCoO₂ lithium-ion batteries during repeated charge–discharge cycling by using digital image correlation, *Measurement* 94 (2016) 759–770. doi:10.1016/j.measurement.2016.09.023.
- [8] L. Willenberg, P. Dechent, G. Fuchs, M. Teuber, M. Eckert, M. Graff, N. Kürten, D. U. Sauer, E. Figgemeier, The development of jelly roll deformation in 18650 lithium-ion batteries at low state of charge, *Journal of The Electrochemical Society* 167 (12) (2020) 120502. doi:10.1149/1945-7111/ABA96D.
- [9] COMSOL Multiphysics v.5.6, COMSOL AB, Stockholm, Sweden, www.comsol.com (2022).
- [10] J. K. Kevorkian, J. D. Cole, Multiple scale and singular perturbation methods, Vol. 114, Springer Science & Business Media, 2012.
- [11] E. Hinch, D. Crighton, M. Ablowitz, S. Davis, A. Iserles, J. Ockendon, P. Olver, *Perturbation Methods*, Cambridge Texts in Applied Mathematics, Cambridge University Press, 1991.
- [12] P. Howell, G. Kozyreff, J. Ockendon, *Applied Solid Mechanics*, Cambridge University Press, 2009.